ISBN: 978-3-95450-247-9 ISSN: 2673-5490 doi: 10.18429/JACoW-IPAC2024-WEPR09

STATUS OF THE SYNCHROTRON RADIATION STUDIES IN THE INTERACTION REGION OF THE FCC-ee

K. D. J. André*, B. Holzer, CERN, Geneva, Switzerland
M. Boscolo, INFN-LNF, Frascati, Italy

Abstract

The FCC-ee is a high-luminosity circular electron-positron collider which will have beam energies spanning 45.6 to 182.5 GeV, and will radiate up to 50 MW of synchrotron radiation power per beam. The lattice design upstream of the interaction point is based on weak dipoles and long straight sections combined with a 30 mrad crossing angle. The optics design provides a flat beam at the IP while integrating an anti-solenoid and detector solenoid. This paper summarizes the design principle and performance of the FCC-ee synchrotron radiation collimation scheme and provides insights into the synchrotron radiation simulations within the interaction region, conducted with BDSIM using the GEANT4 toolkit. Special attention is turned to the complexity of the transverse beam tails, including their width and particle density, representing valuable perspectives for the design of an effective synchrotron radiation collimation system.

INTRODUCTION

FCC-ee is a future high-luminosity and high-energy circular electron-positron collider with a circumference of 90.6 km. To fulfill its physics objectives, its centre-of-mass energy will range from 90 to 365 GeV, and the collider will operate at very high luminosity levels [1]. The machine tunnel is designed with the vision of a subsequent energy-frontier hadron collider FCC-hh [2] in mind. The implementation of a synchrotron radiation collimation scheme within the Interaction Region (IR) is a critical aspect of the Machine-Detector Interface study. This scheme aims at effectively containing synchrotron radiation and minimizing the power deposited near the particle detector. Our study presents simulation results for two operational energies and different beam profiles. At the Z-pole, the FCC-ee will operate in a high-beam current mode, whereas at the highest $t\bar{t}$ energy mode, the IR will face the highest synchrotron radiation photon energies. The main FCC-ee beam parameters for the simulations are listed in Table 1 and the collider layout is presented in Fig. 1.

INTERACTION REGION MODEL

The implementation of the IR model in BDSIM follows the V23 FCC-ee lattice and optics version. It comprises four dipoles upstream of the Interaction Point (IP) and three dipoles downstream of the IP, along with multiple quadrupoles, including the final focus quadrupoles (QC1/2). Additionally, it incorporates a tilted field map consisting of the detector solenoid and anti-solenoids, realistic vacuum chamber models, and includes tungsten synchrotron radiation collimators of 10 cm thickness, and masks of 2 cm thickness.

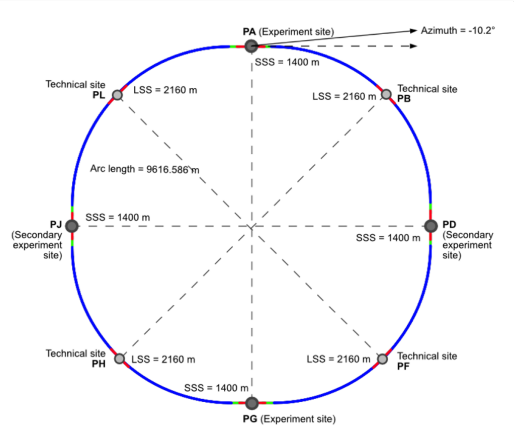

Figure 1: FCC-ee layout with four IPs, where PA, PG, PD, and PJ indicate the experimental sites; PF is the collimation section, PB the injection/extraction section; and PH and PL host the radio-frequency systems.

Synchrotron radiation within the IR has been simulated with BDSIM [4], a program that utilizes the GEANT4 [5] toolkit. The beam line model is translated from MAD-X output files for both operation modes considered into input files for BDSIM. The beam modeling comprises two aspects: the beam core, described by a Gaussian distribution using the beam parameters from Table 1, and the beam tails, represented by a correlated distribution in phase space. The distribution assumes 99% of the particles in the beam core and 1% in the tails, ensuring a particle density similar to the

Table 1: Main FCC-ee Beam Parameters [3]

Operation mode	Z	W	ZH	tt̄
Circumference [km]	90.659			
SR power / beam [MW]	50			
Beam energy [GeV]	45.6	80	120	182.5
Bunches / beam	11200	1780	440	56
Beam current [mA]	1270	137	26.7	4.9
Bunch length σ_z [mm]	15.5	5.41	4.70	2.33
Energy spread σ_δ [%]	0.109	0.109	0.143	0.201
Rms hor. emit. ε_x [nm]	0.71	2.17	0.71	1.59
Rms vert. emit. ε_y [pm]	1.9	2.2	1.4	1.6
Hor. IP beta β_x^* [mm]	110	220	240	800
Vert. IP beta β_y^* [mm]	0.7	1.0	1.0	1.5

* k.andre@cern.ch

ISBN: 978-3-95450-247-9 ISSN: 2673-5490 doi: 10.18429/JACoW-IPAC2024-WEPR09

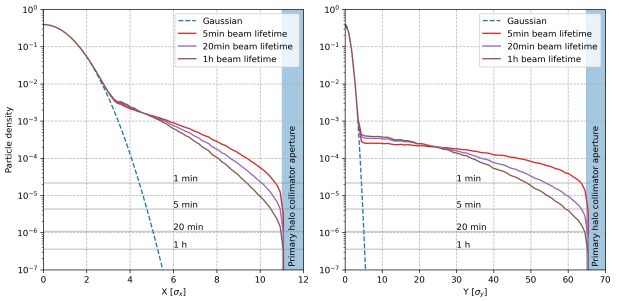

Figure 2: Particle density horizontal (left) and vertical (right) for the beam core and tail distributions for the various beam lifetime used in this study.

sum of two Gaussian distributions as previously used in [6]. Moreover, a beam tail distribution can be extrapolated as a function of beam lifetime [7] as shown in Fig. 2.

The IR design is versatile to accommodate all operation modes with optimized IP beta functions for each running energy, and minimises the synchrotron radiation from the final focus quadrupoles. The crab-waist collision scheme [8, 9] requires a large Piwinski angle, long bunches and small horizontal beam size at the IP. This configuration enables the beams to enter and exit separate beam pipes before the final focus defocusing quadrupole (QC1) closest to the IP. In addition, an asymmetric optics minimises the emission of synchrotron radiation fans into the IR by a softer bending of the incoming beam trajectory. The asymmetric bending also generates the 30 mrad horizontal crossing angle. Stronger dipoles after the IP bring the outgoing beam back near the counter-propagating beam before continuing to the arcs.

SYNCHROTRON RADIATION COLLIMATION SCHEME

The aperture model, presented in Fig. 3, consists of a 30 mm circular aperture throughout the model combined with horizontal winglets to absorb synchrotron radiation and minimize pressure bumps [10] everywhere except for the ±9 m around the IP. From the first final focus quadrupole (QC2) upstream of the IP, the aperture reduces to 20 mm then 15 mm in QC1 and down to 10 mm within the central chamber and vice-versa after the IP. An horizontal SR mask is placed after QC1, at 2.13 m from the IP. A circular mask is foreseen between the final focus quadrupoles, QC2 and QC1, as here the physical aperture is reduced from 20 to 15 mm radius.

The objective of the synchrotron radiation collimation scheme is to protect the vacuum chamber inside the particle detector and to limit the heat load and scattering on the masks closest to the IP. Moreover, the SR collimator apertures must be larger than the beam halo collimator apertures to minimize their interaction with beam halo losses, ultimately limiting the heat load and potential scattering close to the IP.

The beam halo collimation system is installed in section PF (see Fig. 1), and has been studied with particle tracking using the Xtrack-BDSIM coupling simulation framework [11]. Good protection has been demonstrated for halo beam losses assuming a beam lifetime of 5 min at the most critical Z mode [11].

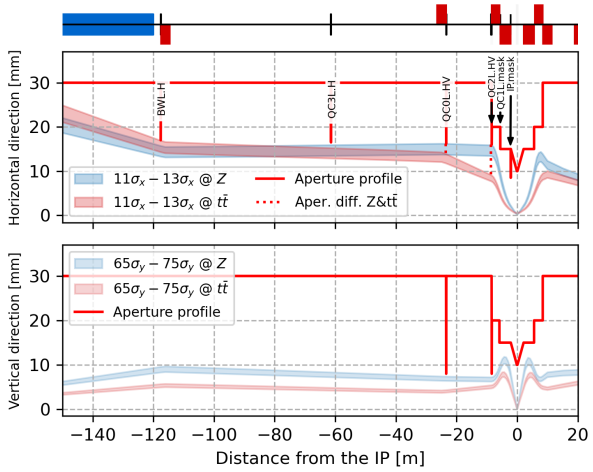

Figure 3: SR horizontal and vertical collimators, and masks.

SR collimators have been implemented in the IR region to intercept synchrotron radiation upstream of the IR. Their positions are shown in Fig. 3 in which the blue and red filled curves highlight the aperture corresponding to the primary and secondary beam halo collimators for the Z and $t\bar{t}$ energies respectively. There are six SR collimators, four horizontal and two vertical, and two masks. While SR collimators and beam halo collimators have minimal interference, tracking simulations of beam halo losses were performed including the SR collimators, with the results presented in Ref. [12].

SIMULATION RESULTS

The main sources of synchrotron radiation background in the IR come from the last dipole magnets before the IP, the solenoid fringe field, and the final focus quadrupoles. Simulations have shown that the synchrotron radiation power deposition increases near the IP and beyond as the transverse beam tails widen. The transverse beam tails are difficult to predict and depend on the stored beam conditions. Therefore several beam lifetimes have been considered and this paper focuses on the least optimistic lifetime of 5 min.

Simulations indicated that synchrotron radiation caused by the particles in the beam core from the last dipole magnet onwards can reach the IP. Radiation from the solenoid field will mostly hit the vacuum chamber of the first dipole downstream of the IP. It must be noted that an extraction line (not included in the model) leading to an instrumented beamstrahlung dump is foreseen in this first dipole [13, 14] and the power deposition displayed in this element in Figs. 4 and 5 will therefore be deposited in the dump.

At Z Energy

The 45.6 GeV energy mode features the highest beam current and hence will create a large amount of relatively low energy photons, making the power deposited a crucial parameter for the cooling assessment.

ISBN: 978-3-95450-247-9 ISSN: 2673-5490 doi: 10.18429/JACoW-IPAC2024-WEPR09

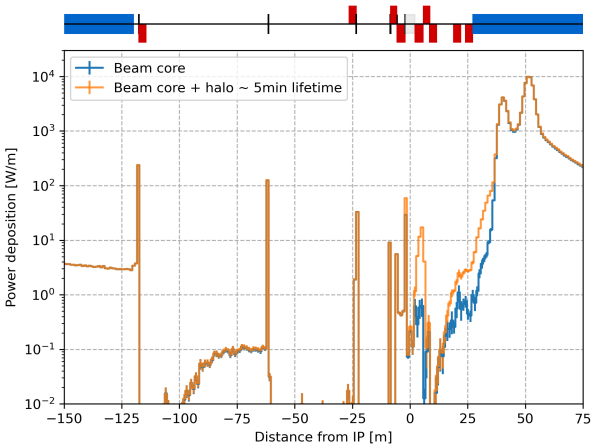

Figure 4: SR power deposition, at Z energy, from s=-150 m to 75 m around the IP. Each bin represents one metre.

Synchrotron radiation from the beam core, represented in blue in Fig. 4, delivers less than a Watt of power deposition in the detector beam pipe. A more precise power deposition is depicted in Fig. 6. The mask effectively intercepts radiation that would otherwise hit the central chamber. Moreover, synchrotron radiation from the beam tails only increases the power deposition beyond 2 m from the IP.

The synchrotron radiation collimation, while respecting the collimation hierarchy, effectively contains the power deposition to specific locations, mitigating the power deposition in the vacuum chamber and near the IP. Although synchrotron radiation from the transverse tail adds heat load onto the mask nearest to the IP, it mostly traverses the central chamber, depositing power downstream of the IP. Overall, the resulting power deposition around the IP is small, dominated by wakefield heat load which is extracted by the central chamber cooling by design [15].

At $t\bar{t}$ Energy

At the $t\bar{t}$ energy the beam current reduces, conserving the total synchrotron radiation power, albeit with increased

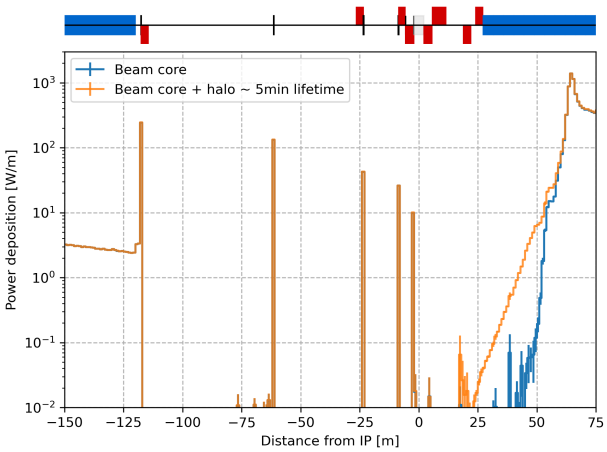

Figure 5: SR power deposition, at $t\bar{t}$ energy, from s=-150 m to 75 m around the IP. Each bin represents one metre.

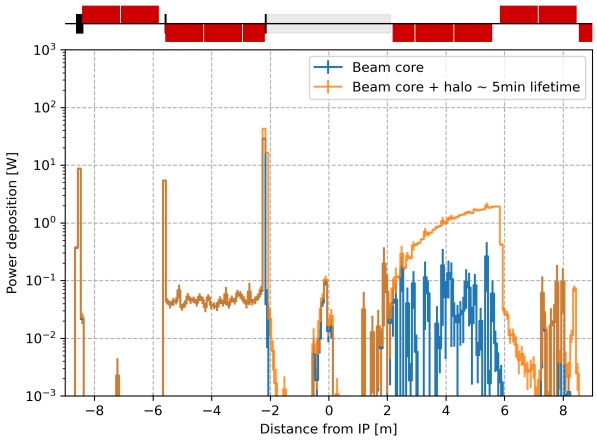

Figure 6: SR power deposition, at Z energy, for ±9 m around the IP. Each bin represents 10 cm.

photon energy. Weak dipoles and quadrupoles upstream the final focus quadrupoles ensure the smallest possible critical energy for the synchrotron radiation generated upstream of the IP.

Synchrotron radiation from the beam core, represented in blue in Fig. 5, displays minimal power deposition near the particle detector, with most of the radiation from upstream of the IP contained in the SR collimation or propagating through the central chamber. The synchrotron radiation collimation, while respecting the collimation hierarchy, confines power deposition to collimator and mask locations. Synchrotron radiation from the transverse beam tails mainly adds heat load onto the mask and downstream of the IP. In summary, the resulting power deposition due to synchrotron radiation from the beam core and tails remains minimal close to the IP, proving the effectiveness of the collimation scheme.

CONCLUSIONS

A synchrotron radiation collimation scheme has been successfully implemented within a complete interaction region model in BDSIM, based on the V23 FCC-ee lattice version, including a tilted solenoid field map and realistic vacuum chamber models.

The devised collimation scheme effectively protects the central chamber and masks from excessive synchrotron radiation flux, thereby minimizing heat load and scattering near the interaction point. Furthermore, the careful positioning of synchrotron radiation collimators also ensures efficient interception and containment of synchrotron radiation upstream of the interaction point.

Simulation results reveal that the additional power deposition around the interaction point is manageable by the cooling capacity foreseen, for both Z and $t\bar{t}$ operational modes.

The expected detector backgrounds from synchrotron radiation have been preliminarily evaluated in Key4HEP, and is reported elsewhere [16] with low occupancy rates, below 1%, observed in the sub-components of the detector.

ISBN: 978-3-95450-247-9 ISSN: 2673-5490 doi: 10.18429/JACoW-IPAC2024-WEPR09

REFERENCES

[1] A. Abada *et al.*, "FCC-ee: The Lepton Collider: Future Circular Collider Conceptual Design Report Volume 2," *Eur. Phys. J. Spec. Top.*, vol. 228, no. 2, pp. 261–623, 2019. doi:10.1140/epjst/e2019-900045-4

[2] A. Abada *et al.*, "FCC-hh: The Hadron Collider: Future Circular Collider Conceptual Design Report Volume 3," *Eur. Phys. J. Spec. Top.*, vol. 228, no. 4, pp. 755–1107, 2019. doi:10.1140/epjst/e2019-900087-0

[3] K. Oide, "Optics performance, beam lifetime and injection rate," presented at the FCCIS 2023 WP2 Workshop, Rome, Italy, 2023.

[4] L. Nevay *et al.*, "Bdsim: An accelerator tracking code with particle–matter interactions," *Comput. Phys. Commun.*, vol. 252, p. 107 200, 2020. doi:10.1016/j.cpc.2020.107200

[5] J. Allison *et al.*, "Recent developments in Geant4," *Nucl. Instrum. Methods Phys. Res., Sect. A*, pp. 186–225, 2016. doi:10.1016/j.nima.2016.06.125

[6] M. Sullivan, "IR Design Issues for High Luminosity and Low Backgrounds," Frascati, Italy, 2022, paper TUZAT0101. doi:10.18429/JACoW-eeFACT2022-TUZAT0101

[7] M. Sands, "The Physics of Electron Storage Rings: An Introduction," *Conf. Proc. C*, vol. 6906161, pp. 257–411, 1969.

[8] M. Zobov *et al.*, "Test of crab-waist collisions at DAFNE Phi factory," *Phys. Rev. Lett.*, vol. 104, p. 174 801, 17 2010. doi:10.1103/PhysRevLett.104.174801

[9] K. Oide *et al.*, "Design of beam optics for the Future Circular Collider e^+e^--collider rings," *Phys. Rev. Accel. Beams*, vol. 19, p. 111 005, 11 2016. doi:10.1103/PhysRevAccelBeams.19.111005

[10] R. Kersevan, "Vacuum system and photoelectron distributions in the collider," presented at the FCCIS 2023 WP2 Workshop, Rome, Italy, 2023.

[11] A. Abramov *et al.*, "Development of Collimation Simulations for the FCC-ee," in *Proc. IPAC'22*, Bangkok, Thailand, 2022, paper WEPOST016, pp. 1718–1721. doi:10.18429/JACoW-IPAC2022-WEPOST016

[12] G. Broggi *et al.*, "Optimizations and updates on the FCC-ee collimation system design," Nashville, Tennessee, USA, this conference, 2024.

[13] A. Frasca, "Beamstrahlung dump and radiation levels in the experiment irs," presented at the FCC week 2023 conference, London, England, 2023.

[14] M. Boscolo and A. Ciarma, "Characterization of the beamstrahlung radiation at the future high-energy circular collider," *Phys. Rev. Accel. Beams*, vol. 26, p. 111 002, 11 2023. doi:10.1103/PhysRevAccelBeams.26.111002

[15] A. Novokhatski *et al.*, "Estimated heat load and proposed cooling system in the fcc-ee interaction region beam pipe," in *Proc. IPAC'23*, Venice, Italy, 2023, pp. 260–263. doi:10.18429/JACoW-IPAC2023-MOPA092

[16] A. Ciarma *et al.*, "Machine Induced Backgrounds in the FCC-ee MDI Region and Beamstrahlung Radiation," in *Proc. eeFACT'22*, Frascati, Italy, 2022, paper TUZAT0203, pp. 85–90. doi:10.18429/JACoW-eeFACT2022-TUZAT0203